An optical homodyne technique to measure photorefractive-induced phase drifts in lithium niobate phase modulators

Ruey-Ching Twu[1*], Hao-Yang Hong[1], and Hsuan-Hsien Lee[2]

[1]*Department of Electro-Optical Engineering, Southern Taiwan University*
1, Nan-Tai St., Yung-Kang City, Tainan 710, Taiwan, R.O.C.
[2]*Department of Electrical Engineering, Southern Taiwan University*
1, Nan-Tai St., Yung-Kang City, Tainan 710, Taiwan, R.O.C.
[*] *rctwu@mail.stut.edu.tw*

Abstract: In this paper, we develop an optical measurement system with capabilities of phase unwrapping, real-time and long-term monitoring for measuring a phase drift caused by photorefractive effects in lithium niobate phase modulators. To extract the phase-drift variations, the measurement setup uses a homodyne interferometer with a phase modulation and a Fast Fourier Transform (FFT) demodulation scheme. The phase-drift characteristics of a traditional Ti-indiffused and a Zn-indiffused phase modulator have been investigated under different applied voltages and throughput powers. These experiments were conducted as a proof-of-concept to demonstrate that the apparatus worked successfully to measure the phase drift of a device in the presence of photorefractive effects. The results indicate that the Zn-indiffused phase modulators have better photorefractive stability than the Ti-indiffused phase modulators.

OCIS codes: (120.4640) Optical instruments; (160.3730) Lithium niobate.

References and links

1. R. C. Alferness, "Electrooptic guided-wave device for general polarization transformations," IEEE J. Quantum Electron. **17**, 965-969 (1981).
2. T. Kawazoe, K. Satoh, I. Hayashi, and H. Mori, "Fabrication of integrated-optic polarization controller using z-propagating Ti-$LiNbO_3$ waveguides," J. Lightwave Technol. **10**, 51-56 (1992).
3. M. H. Chou, I. Brener, M. M. Fejer, E. E. Chaban, and S. B. Christman, "1.5-μm-band wavelength conversion based on cascaded second-order nonlinearity in $LiNbO_3$ waveguides," IEEE Photon. Technol. Lett. **11**, 653-655 (1999).
4. G. Zhang, G. Zhang, S. Liu, J. Xu, G. Tian, and Q. Sun, "Theoretical study of resistance against light-induced scattering in $LiNbO_3$:M (M = Mg^{2+},Zn^{2+},In^{3+},Sc^{3+}) crystals," Opt. Lett. **22**, 1666-1668 (1997).
5. Y. Kong, J. Wen, and H. Wang, "New doped lithium niobate crystal with high resistance to photorefraction–$LiNbO_3$: In," Appl. Phys. Lett. **66**, 280-281 (1995).
6. P. Minzioni, I. Cristiani, J. Yu, J. Parravicini, E. P. Kokanyan, and V. Degiorgio, "Linear and nonlinear optical properties of Hafnium-doped lithium-niobate crystals," Opt. Express **15**, 14171-14176 (2007).
7. C. H. Huang and L. McCaughan, "980-nm-pumped Er-doped $LiNbO_3$ waveguide amplifier: a comparison with 1484-nm pumping," J. Selected Topics in Quantum Electron. **2**, 367-372 (1996).
8. L. Ming, C. B. E. Gawith, K. Gallo, M. V. O'Connor, G. D. Emmerson, and P. G. R. Smith, "High conversion efficiency single-pass second harmonic generation in a zinc-diffused periodically poled lithium niobate waveguide," Opt. Express **13**, 4862-4868 (2005).
9. T. Fujiwara, R. Srivastava, X. Cao, and R. V. Ramaswamy, "Comparison of photorefractive index change in proton-exchanged and Ti-diffused $LiNbO_3$ waveguides," Opt. Lett. **18**, 346-348 (1993).
10. O. Eknoyan, H. F. Taylor, W. Matous, and T. Ottinger, "Comparison of photorefractive damage effects in $LiNbO_3$, $LiTaO_3$, and $Ba_{1-x}Sr_xTi_yNb_{2-y}O_6$ optical waveguides at 488 nm wavelength," Appl. Phys. Lett. **71**, 3051-3053 (1997).
11. R. A. Becker, "Thermal fixing of Ti-indiffused $LiNbO_3$ channel waveguides for reduced photorefractive susceptibility," Appl. Phys. Lett. **45**, 121-123 (1984).
12. H. Nagata, K. Kiuchi, S. Shimotsu, and J. Ogiwara, "Estimation of direct current bias and drift of Ti: $LiNbO_3$ optical modulators," J. Appl. Phys. **76**, 1405-1408 (1994).

#92237 - $15.00 USD Received 29 Jan 2008; revised 11 Mar 2008; accepted 11 Mar 2008; published 14 Mar 2008

13. S. Thaniyavarn, "Wavelength independent, optical damage immune z-propagation $LiNbO_3$ waveguide polarization converter," Appl. Phys. Lett. **47**, 674-677 (1985).
14. M. Levesque, M. Têtu, P. Tremblay, and M. Chamberland, "A novel technique to measurement the dynamic response of an optical phase modulator," IEEE Trans. Instrum. Meas. **44**, 952-957 (1995).
15. B. Sepúlveda, G. Armelles, and L. M. Lechuga, "Magneto-optical phase modulation in integrated Mach-Zehnder interferometer sensors," Sens. Actuators A-Phys. **134**, 339-347 (2007).
16. V. S. Sudarshanam and K. Srinivasan, "Linear readout of dynamic phase change in a fiber-optic homodyne interferometer," Opt. Lett. **14**, 140-143 (1989).
17. R. C. Twu, H. H. Lee, H. Y. Hong, and C. Y. Yang, "A novel Zn-indiffused mode converter in x-cut lithium niobate," Opt. Express **15**, 15576-15582 (2007).
18. E. P. Kokanyan, L. Razzari, I. Cristiani, V. Degiorgio, and J. B. Gruber, "Reduced photorefraction in hafnium-doped single-domain and periodically poled lithium niobate crystals," Appl. Phys. Lett. **84**, 1880-1882 (2004).
19. M. Carrascosa, J. Villarroel, J. Carnicero, A. Garcia-Cabanes, and J. M. Cabrera, "Understanding light intensity thresholds for catastrophic optical damages in $LiNbO_3$," Opt. Express **16**, 115-120 (2008).
20. M. Falk, Th. Woike, and K. Buse, "Reduction of optical damage in lithium niobate crystals by thermo-electric oxidation," Appl. Phys. Lett. **90**, 251912 (2007).

1. Introduction

Lithium niobate (LN) waveguide devices exhibiting excellent characteristics of electro-optic (EO) and nonlinear optic (NLO) can provide various functions of phase modulation, polarization rotation, and wavelength conversion [1-3]. To increase the bandwidth in optical communication systems, the wavelength channels of input light sources can be expanded by using the periodically poled LN structures via difference-frequency-generation and sum-frequency-generation mechanisms, based on the NLOs [3]. The output signal intensity as well as wavelength conversion efficiency is dependent on the optical intensities of pumping lights. However, higher pumping powers and shorter conversion wavelengths easily make the unstable phase-matching conditions. Because the bounded electrons can be optically excited from the Fe^{2+} sites, due to the photorefractive effects in LN materials [4], the photo-excited electrons drift-out to the edge of the waveguides. Usually, the drift directions of the carries are anisotropic that are dependent on the substrate geometry and applied voltage. The accumulated carriers can further produce an electric field to modulate the local refractive index through an electro-optic (EO) effect. Therefore, the propagation phase of a guiding wave is modulated accordingly. The induced phase changes will make the output powers unstable in an EO modulator. Thus, it needs additional feedback control to maintain stable DC-bias conditions. To enhance the resistance to photorefractive effects, the LN crystals can be doped with various dopants such as Mg, Zn, Hf, and In elements during crystal growth [4-6]. Besides, a metal-oxide or a metallic Zn-indiffused waveguide has been studied more extensively, due to the lower diffusion temperature as well as higher photorefractive stability, than the conventional Ti-indiffused waveguides [7, 8]. Therefore, it is essential to develop a real-time and long-term monitoring instrument for measuring the dynamic behaviors of the photorefractive effect in the LN waveguide devices.

In the past decade, the phase drifts that resulted from photorefractive effects can be measured by using pumping (shorter wavelengths and higher intensities) and probing (longer wavelengths and lower intensities) methods [9, 10]. The photorefractive-induced power variations were observed in the passive waveguides by utilizing suitable optical arrangements such as Mach-Zehnder and Fabry-Perot interferometers. However, these arrangements need careful alignments for multiple input light sources. Besides, the open-loop and closed-loop schemes for monitoring the power variations of EO modulators have been employed to study the phase-drift characteristics under different applied voltages and process conditions [11, 12]. Among them, most of the evaluated modulators were fabricated in *y*-propagation or *x*-propagation substrates by utilizing r_{33} electro-optic coefficient for high-speed applications. However, the *z*-propagation devices, such as mode converters and phase modulators, are essential for fabrications of optical-polarization controller and scrambler. Moreover, the *z*-propagation phase modulators suffer from less photorefractive effects than the other *y*-

#92237 - $15.00 USD Received 29 Jan 2008; revised 11 Mar 2008; accepted 11 Mar 2008; published 14 Mar 2008

propagation or *x*-propagation ones [13]. These advantages are useful to make a compact polarization modulator for optical metrology in the visible region.

In this paper, we develop an optical measurement system with capabilities of phase unwrapping, real-time and long-term monitoring for measuring phase drifts of LN phase modulators due to photorefractive effects. The experimental setup uses a homodyne interferometer based on phase-modulation and Fast-Fourier-Transform (FFT) demodulation schemes, in which they have been successfully demonstrated in optical metrology for both common-path and splitting-path interferometers [14-16]. A comparison of phase drifts between the Zn-indiffused (ZI) and the Ti-indiffused (TI) phase modulators, fabricated in the same x-cut/z-propagation substrates, are further evaluated at a wavelength of 0.632 μm by using the proposed measurement system. The results show that the ZI phase modulators have better photorefractive stability than the TI ones. Eventually, the proposed metrology shows that it can provide a useful estimation for a reliability test of phase drift as it has been used in LN phase modulators.

2. Experimental setup and measurement principles

Figure 1 shows a device structure and an experimental setup of the proposed method for real-time monitoring the phase drifts of LN phase modulators. An x-cut/y-propagation phase modulator consisting of a channel waveguide and a pair of electrodes, which placed parallel and adjacent to the channel, was used to evaluate the photorefractive effects under various applied voltages and throughput powers. The phase delay between the TE- and TM-waves ($\phi_{\text{TE-TM}}$) can be modulated by driving electric signals over the electrodes through EO coefficients of r_{22} and r_{12}. The input powers can be controlled by changing the relative transmittance angles between polarizers of PL1 and PL2. By controlling the relative angles between PL2 and the principle axis of half-wave plate (λ/2 WP), a linear polarization oriented at an angle of 45° relative to the crystal *x*-axis is launched in the phase modulator via an object lens L1 (40×). The output beam was received by an amplified photo-detector (PD) after passing through a coupling object lens L2 (40×), a pinhole (Pin), and an analyzer (AL) oriented at −45°.

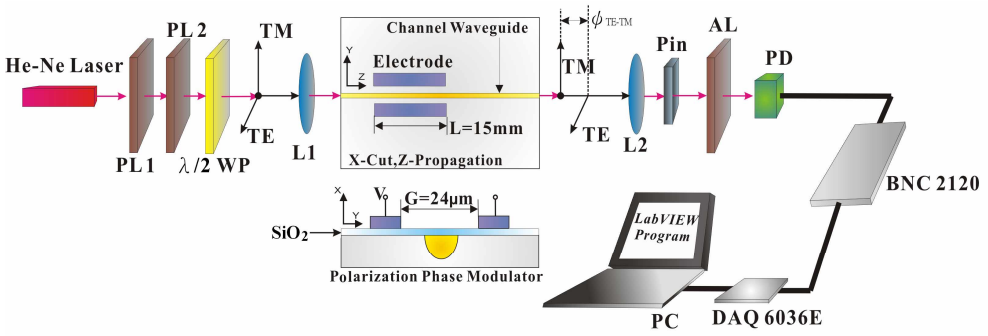

Fig. 1. A schematic of the experimental setup for measuring a phase drift of a phase modulator.

Similar to the derived equations in [14], in the case of a sinusoidal voltage over the phase modulator, the normalized output signal P_{out} can be expressed as

$$P_{out} = \gamma_{TE}^2 + \gamma_{TM}^2 + 2\gamma_{TE}\gamma_{TM}\cos\left[\beta\sin(2\pi ft) + \phi\right] \quad (1)$$

where the values of γ_{TE} and γ_{TM} are dependent on the polarization-dependent insertion loss of channel waveguides, and the transmittance angles between the polarizers of PL2 and AL. The f and β are frequency and modulation depth of the applied voltages, respectively; ϕ is the phase variations. The β is further represented by

#92237 - $15.00 USD Received 29 Jan 2008; revised 11 Mar 2008; accepted 11 Mar 2008; published 14 Mar 2008

$$\beta = \frac{V_{ac}}{V_{\pi}}\pi \tag{2}$$

where V_{ac} is the applied peak-to-peak amplitudes of AC voltages; V_{π} is the switching voltages for a π phase-shift between TE- and TM-waves in the phase modulator. The ϕ can be written

$$\phi = \Delta\phi + \Delta\phi^{PR} \tag{3}$$

where $\Delta\phi$ is a static phase-difference between propagating TE- and TM-modes due to different boundary conditions; the time-varying phase drift $\Delta\phi^{PR}$, caused by the photorefractive effects is expressed by

$$\Delta\phi^{PR} = \frac{4\pi}{\lambda} L n_o^3 r_{22} \Gamma E_{PR} \tag{4}$$

where λ is the optical wavelength, L is the channel length, n_o is the ordinary refractive index of substrate, Γ is the normalized electro-optic overlap integral, and E_{PR} is the photorefractive-induced electric field. According to Eq. (1), the output signal can be further expanded in Fourier series, resulting:

$$P_{out} = \gamma_{TE}^2 + \gamma_{TM}^2 + 2\gamma_{TE}\gamma_{TM}\sum_{k=-\infty}^{\infty} J_k(\beta)\cos(\phi + 2\pi k f t) \tag{5}$$

where $J_k(\beta)$ is the Bessel function of order k with an index factor of β. The amplitudes of discrete frequency components can be obtained by using Fast Fourier Transform (FFT) technique. The first and second harmonics are I_1 and I_2, respectively:

$$I_1 = 4\gamma_{TE}\cdot\gamma_{TM}\sin(\phi)J_1(\beta) \tag{6}$$

$$I_2 = 4\gamma_{TE}\cdot\gamma_{TM}\cos(\phi)J_2(\beta) \tag{7}$$

According to Eq. (6) and Eq. (7), the values of ϕ can be calculated by the following equation

$$\phi = \tan^{-1}\left(\frac{I_1\cdot J_2(\beta)}{I_2\cdot J_1(\beta)}\right) \tag{8}$$

After a division operation in Eq. (8), the polarization-dependent factors of γ_{TE} and γ_{TM} as shown in both Eq. (6) and Eq. (7) can be canceled out. Therefore, the precision of measurements is mainly dependent on the values of harmonic signals and β. For data acquisition and analysis, we use a PC-based system operating in a LabVIEW environment (version 7.0, National Instrument). The received data from the photo-detector was connected to a lap-top personal computer through a multichannel signal box (BNC-2120, National Instrument), and a data-acquisition-card (DAQ-6036E, National Instrument). Finally, the real-time and long-term monitoring can be successfully displayed with the designed LabVIEW front panel. The received records also can be saved to an external file for further analysis.

3. Estimation on the validity of the proposed measurement systems

Several experiments are conducted to validate the performance of the optical arrangement proposed in Fig.1. A Zn-strip of 4 μm-wide, and 35 nm-thick with predeposition Ni film of 6 nm was performed with thermal diffusion of 850°C for 150 min to obtain the single-mode operation. After thermal diffusion and end faces polished, a silicon dioxide (SiO_2) buffer layer of 300 nm was deposited. Then an Al electrode of thickness 300 nm was deposited and patterned. The gap width G between parallel electrodes is 24 μm, and the electrode length L is 15 mm. The received optical signal and the corresponding analyzed FFT spectrum are shown in Figs. 2(a) and 2(b), respectively. In the case of short-period and low-power operations, the photorefractive effects can be ignored. To ensure a validation of the proposed method, we input a sinusoidal voltage V_{ac} over the waveguide electrodes of ZI phase modulator with a peak-to-peak value of 10 V and a frequency of 100 Hz at a throughput power of about 5 μW. At the same time, a slow sinusoidal voltage with frequency of 0.01 Hz is applied over the

#92237 - $15.00 USD Received 29 Jan 2008; revised 11 Mar 2008; accepted 11 Mar 2008; published 14 Mar 2008

same electrodes to produce the simulated phase-drift $\Delta\phi^{PR}$ as expressed in Eq. (4). Thus, the induced phase variations are also sinusoidal-like curves through EO effects. Because the extracted phase values after an operation of arctan are within in a range from 0 to $\pi/2$, it will possibly limit the dynamic measurement range in a real situation. Figure 2(c) gives the simulated phase variations with a phase ambiguity near $\pi/2$ (~1.57 rad). The phase ambiguity can be solved by using a phase-unwrapping technique performed with LabVIEW programs, as shown in Fig. 2(d).

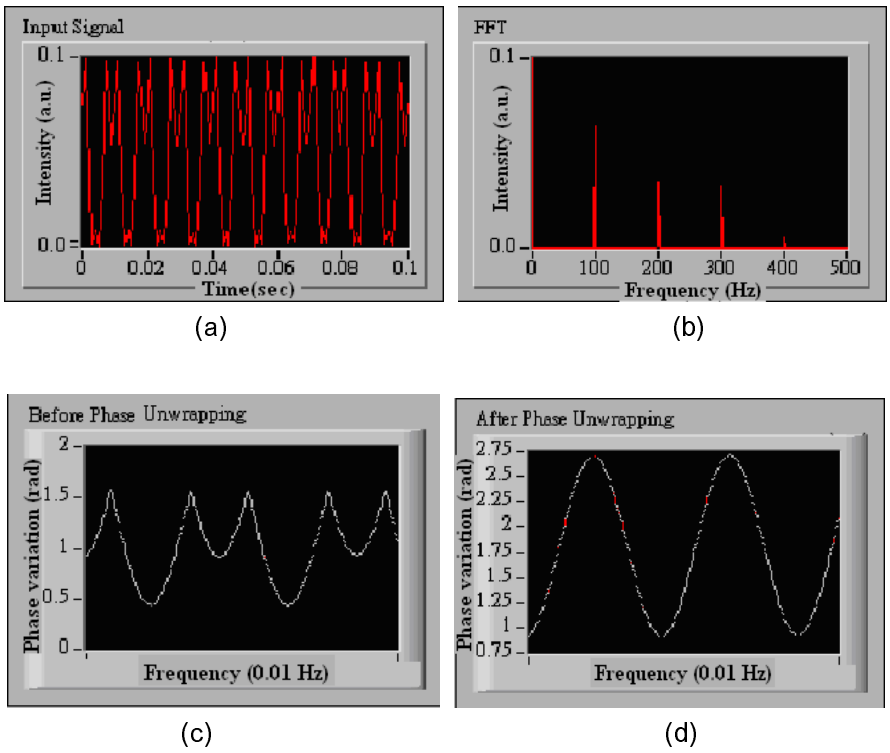

Fig. 2. LabVIEW-based front panel for real-time and long-term monitoring to the received and calculated signals: (a) the measured optical signal, (b) the analyzed FFT spectrum, (c) the measured phase variations with a phase ambiguity, and (d) the phase-unwrapping signal.

According to Eq. (8), the measurements' precision of ϕ are dependent on the chosen values of β. A slow triangular voltage (f = 0.01 Hz, peak-to-peak voltage = 2 V) was used for the input simulated voltage, and the comparisons of linearity between input simulated voltages and corresponding phase drifts for different values of β are shown in Fig. 3. Because the simulated $\Delta\phi^{PR}$ is a linear function of the applied voltage, in the ideal case, the phase changes versus the applied voltages should be a straight line (black trace) in the observed quarter period of triangular signal. At the same input voltage signals, if the values of β are not correct parameters (blue and red traces) for modulation depths, the calculated results are bending curves in the full measurement ranges. In contrast, the best value of β = 2.6 (green trace) is automatically determined by using the prompt LabVIEW programs, where it can obtain more parallel regions of about 80% compared to the ideal case in the dynamic range. The curves bending are only near the peak regions of triangular voltages due to the abrupt phase changes. Besides, the calculated V_π is 12.1 V based on the measured β and Eq. (2).

#92237 - $15.00 USD Received 29 Jan 2008; revised 11 Mar 2008; accepted 11 Mar 2008; published 14 Mar 2008

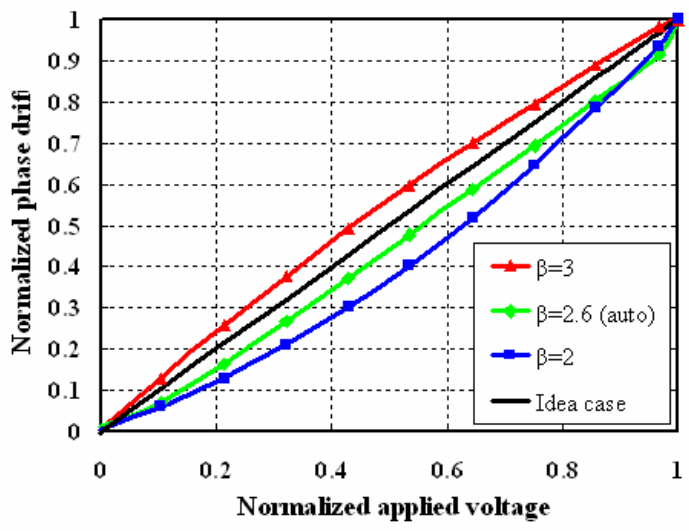

Fig. 3. Linearity between simulated voltages and induced phase drifts for different values of β.

The dependence of phase variations on the alignment angles of the analyzer is shown in Fig. 4. The dynamical ranges of phase variation are about 1.11, 1.12, and 1.15 rad for the corresponding AL angles −50°, −45°, and −40°, respectively. It shows that the AL angles are tolerant to make the optical setup easy. These properties also indicate that the polarization-dependent insertion loss regarding the end-face coupling and guided-wave propagating do not induce serious measurement errors. According to the experimental results, the proposed method of using the setup of homodyne interferometer, the FFT analysis, and the LabVIEW platform can solve the problems of the ambiguity and fading of phase-drift variations measuring in the phase modulators [11]. In addition, the detection of the phase change is immune to the intensity changes caused by the polarization-dependent insertion loss of channel waveguides, and slight misalignments of the optical components.

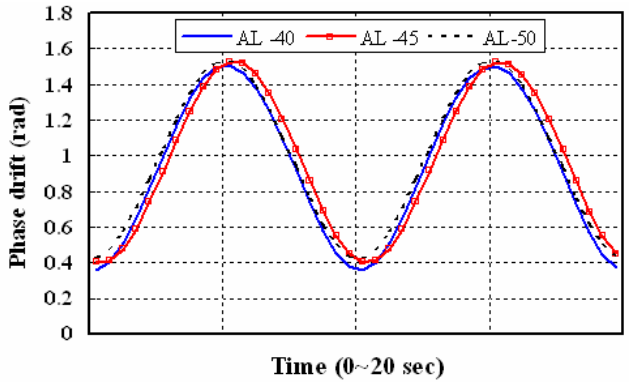

Fig. 4. Dependence of simulated phase variations on the angles of the analyzer (AL).

#92237 - $15.00 USD Received 29 Jan 2008; revised 11 Mar 2008; accepted 11 Mar 2008; published 14 Mar 2008

4. Comparisons of phase drift between the ZI and TI phase modulators

To compare the characteristics of phase drift between the ZI and TI phase modulators on the same congruent pure LN substrates. A single-mode TI waveguide for both TE- and TM-polarizations was fabricated by using a Ti-strip of 4 μm-wide, and 32 nm-thick, which was thermally diffused at 1000°C for 4 h in a furnace with the oxygen ambient. There, the electrode structures of the TI modulator are the same as in the ZI modulator. Figure 5 gives the phase-drift measurements of the TI and ZI phase modulators under various applied DC voltages, at throughput powers of 5 μW measuring after the pinhole, with the same input AC modulation signals (V_{ac} = 10 V; f = 100 Hz) in an observation period of 10 min. In general, the phase modulation of f = 100 Hz is much faster the response of the photorefractive reactions, which is typically in the order of minutes [11]. The maximum phase drifts of the TI modulator are about 0.4 rad for different DC voltages, as shown in Fig. 5(a). In contrast, the maximum phase drifts of the ZI modulator are 0.17, –0.17 and 0.22 rad for DC voltages 10, 0, and –10 V, respectively, as shown in Fig. 5(b).

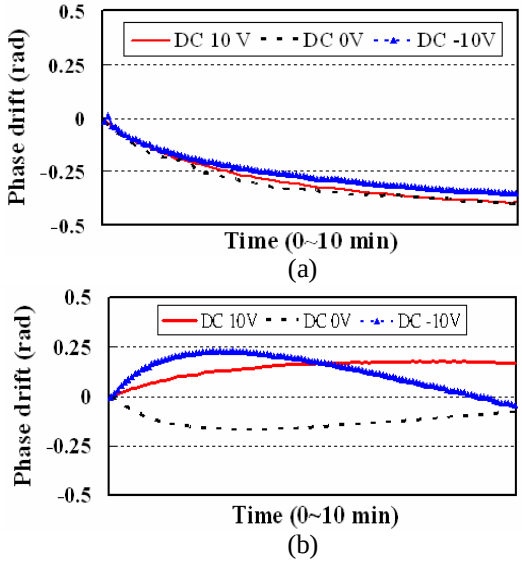

Fig. 5. Comparison of phase drift as a function of illuminating time under different applied DC voltages at a throughput power of 5 μW: (a) TI phase modulator and (b) ZI phase modulator.

#92237 - $15.00 USD Received 29 Jan 2008; revised 11 Mar 2008; accepted 11 Mar 2008; published 14 Mar 2008

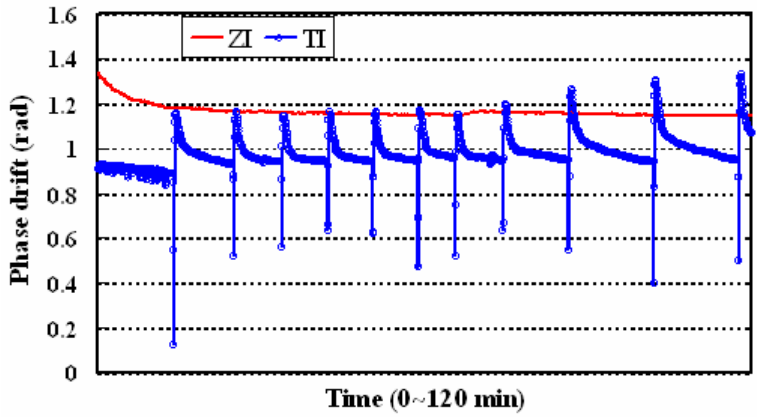

Fig. 6. Comparison of phase drifts as a function of illuminating time for the TI and ZI phase modulators at a throughput power of 25 μW.

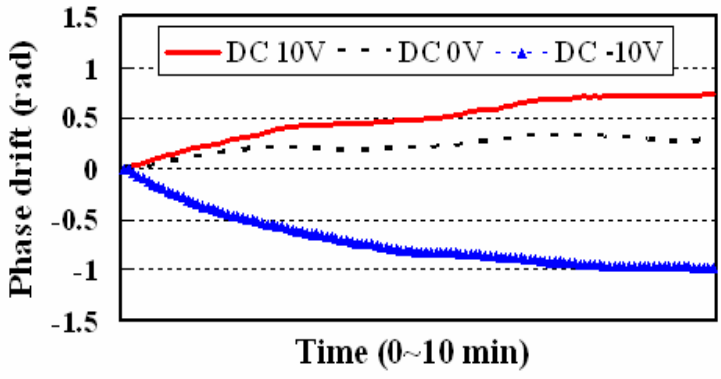

Fig. 7. Phase drifts of the ZI phase modulator as a function of illuminating time under different applied DC voltages at a throughput power of 50 μW.

By increasing the input powers, when the throughput power is about 25 μW, the comparisons of the TI and ZI modulators on the phase drifts versus irradiating time are shown in Fig. 6. At the same AC voltages and DC bias of 0 V, the TI modulator (blue trace) shows some abrupt changes in the measurement period of 120 min. These characteristics are probably caused by the unstable power-handing due to the photorefractive effects in the channel waveguides under higher irradiated powers [17]. Otherwise, the ZI one (red trace) is gradually decreased in the initial period of about 20 min. The maximum phase drifts are about 0.18 rad. Then, it maintains a near-stable saturated phase for 120 min. Figure 7 shows the phase drifts of ZI modulators under a throughout optical power of 50 μW for different DC-biased voltages in an observation period of 10 min. The maximum phase drifts are 0.79, 0.32 and −0.98 rad for DC voltages 10, 0, and −10 V, respectively. The previous measurements demonstrate that the phase changes as a function of irradiated time are exponential-like curves in the low throughout power region (< 25 μW) for both ZI and TI waveguides. These tendencies are similar to the reported results [12, 18]. Recently, the light-induced phase jumps attributed to the catastrophic optical damage have been reported [19]. Besides, another report has mentioned that the highly input powers over some critical values easily cause unstable data of phase changes by using the typical Senarmont compensation method [20]. Although their experiments were demonstrated in the bucks [19, 20], we believe that these intrinsic material properties of photorefractive will be enhanced in the channel waveguide due to a higher power density within a guided mode. It may be possible to conceptually explain the

#92237 - $15.00 USD Received 29 Jan 2008; revised 11 Mar 2008; accepted 11 Mar 2008; published 14 Mar 2008

phase jumps of TI waveguides under higher irradiated powers (throughout optical power > 25 μW) in our experiments. In comparison with the conventional TI modulators, the ZI modulators can provide more stable operations due to less photorefractive sensitivity at 0.632 μm wavelength. In the same ZI modulators, the higher DC voltages and input powers will also increase the phase drifts.

5. Conclusions

We have successfully demonstrated a simple and novel method to measure the phase drift caused by the photorefractive effects in LN phase modulators, for the first time. The signal processing is performed with LabVIEW-based hardware and software, which can effectively integrate the necessary functional instruments in comparison with traditional arrangements. Moreover, this proposed method can provide advantages of phase-unwrapping, real-time and long-term monitoring, which also can give more details for studying the dynamic behaviors of photo-excited carriers in the waveguides, under different DC biases and input optical powers. Finally, the compared results also indicate that the Zn-indiffused modulator is able to handle higher optical powers than the Ti-indiffused modulator, without suffering from photorefractive effects on the optical phase at 0.632 μm wavelength.

Acknowledgments

This work was supported in part by the National Science Council, Taiwan, R.O.C., under Grants NSC 96-2221-E-218-026 and NSC 96-2622-E-218-017-CC3.

#92237 - $15.00 USD Received 29 Jan 2008; revised 11 Mar 2008; accepted 11 Mar 2008; published 14 Mar 2008